Supporting Information

GSH-Depleting Metal-Polyphenol-Network Nanoparticles with Dual Enzyme Activities Endow Enhanced Ferroptosis

Wen-Xin Zhang [a], You Li [b], Di Ke [a], Yi-Ru Gao [a], Teng Fei [b], Guo-Qing Wang [b], Yang Shu [*a], Jian-Hua Wang* [*a]*

a Department of Chemistry, College of Sciences, Northeastern University, Box 332, Shenyang 110819, China

b College of Life and Health Sciences, Northeastern University, Shenyang 110819, China

*Corresponding author

E-mail address: shuyang@mail.neu.edu.cn (Y. Shu), jianhuajrz@mail.neu.edu.cn (J.H. Wang).

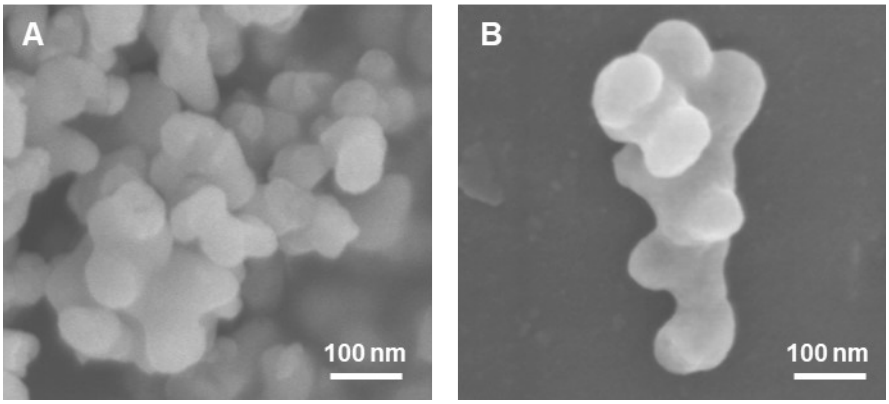

Figure S1. SEM images of Ce-aMOFs (A) and MEFs (B) nanoparticles, with a scale bar of 100 nm.

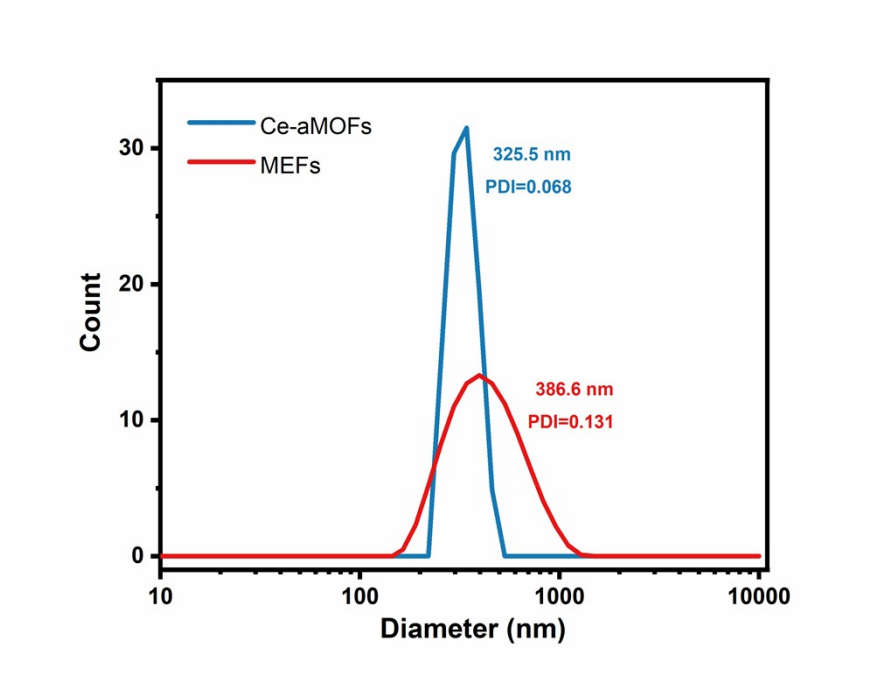

Figure S2. DLS analysis results for Ce-aMOFs and MEFs (100 μg mL^{-1}, n=3).

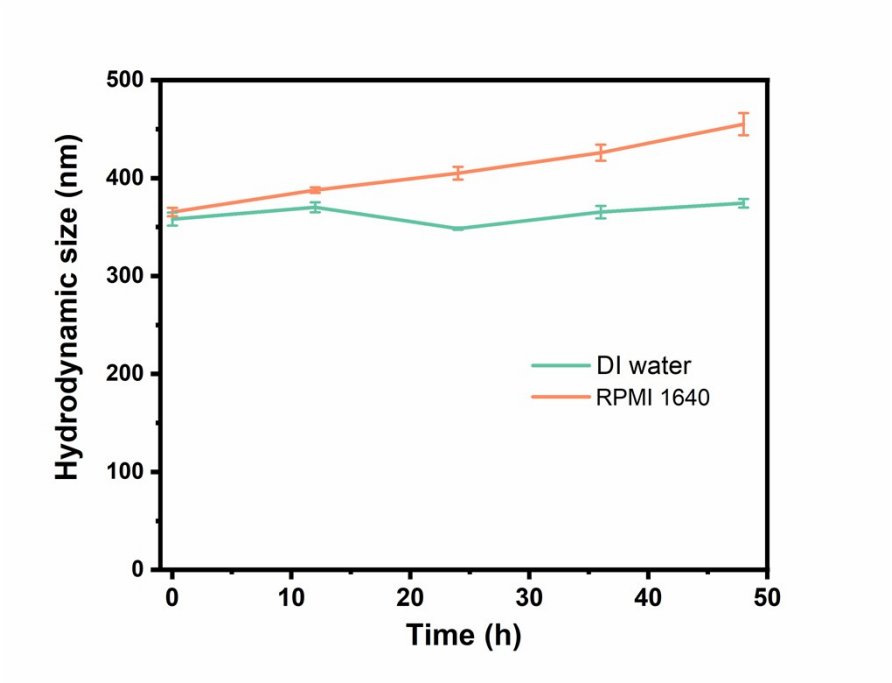

Figure S3. Stability of MEFs in DI water and RPMI 1640 basic medium at room temperature, (n=3).

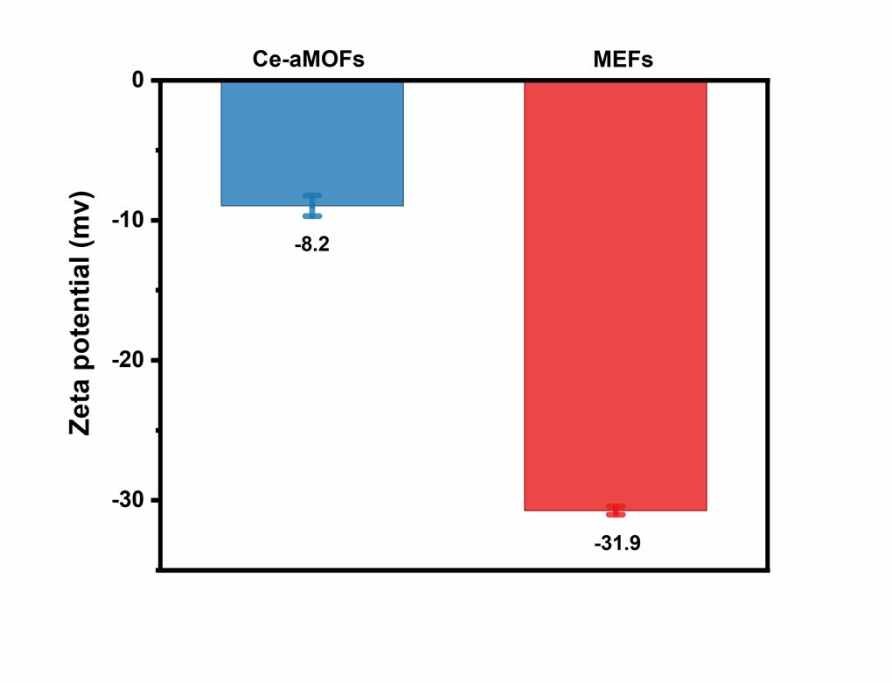

Figure S4. Zeta potentials of Ce-aMOFs and MEFs at pH 7.4 (n=3).

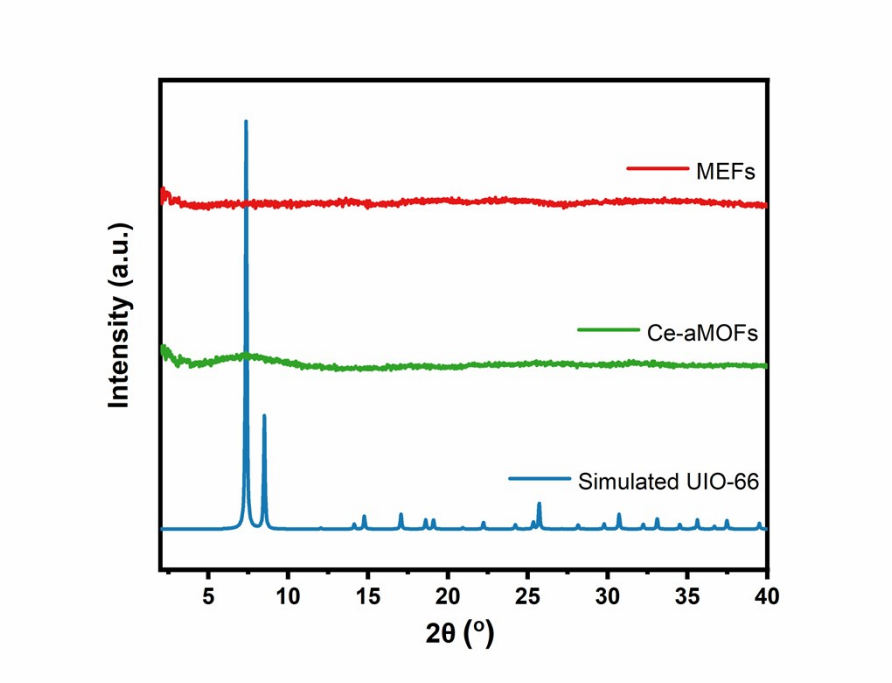

Figure S5. XRD patters for Ce-aMOFs and MEFs.

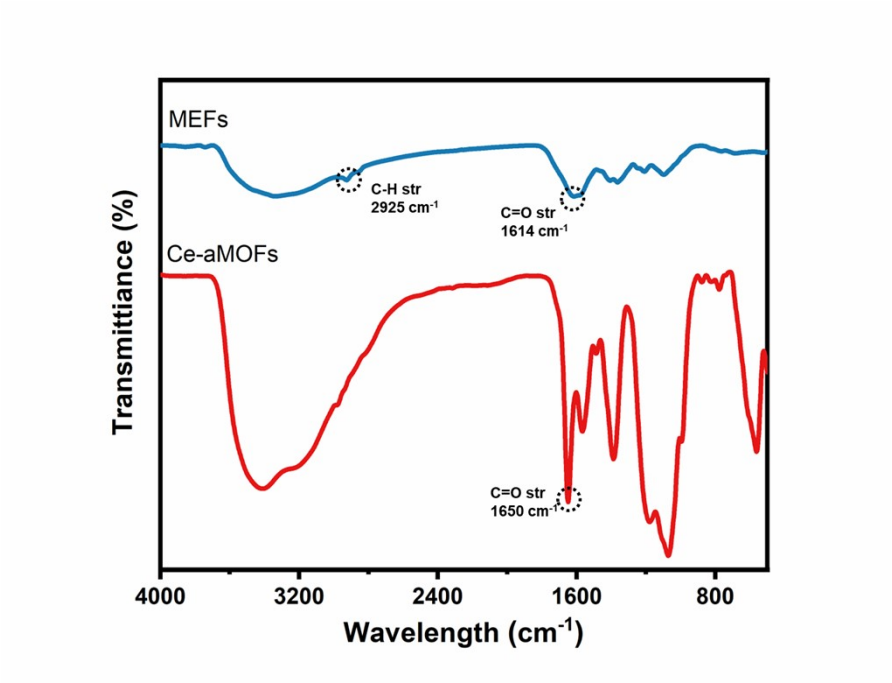

Figure S6. FT-IR spectra of Ce-aMOFs and MEFs.

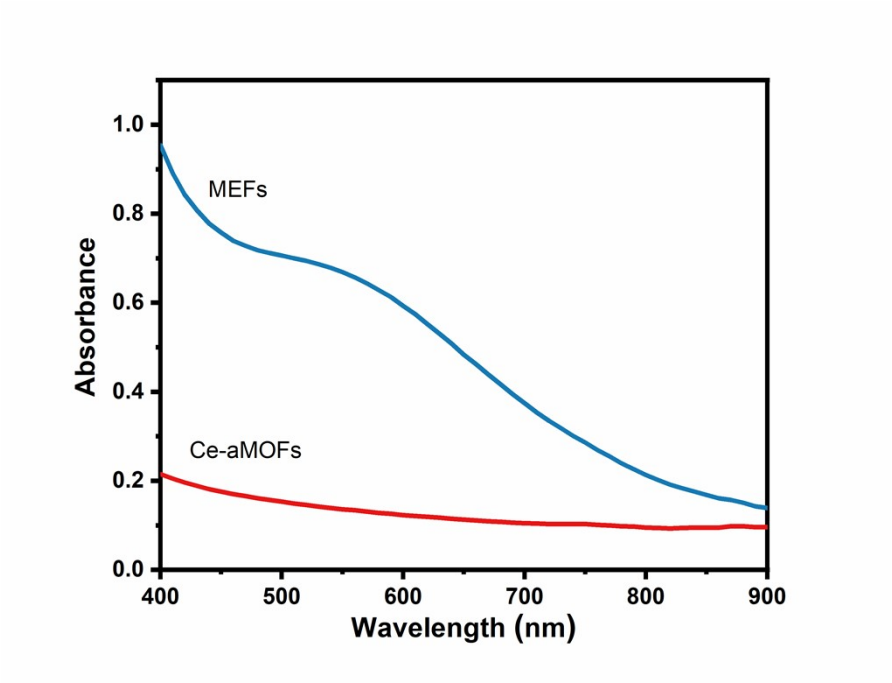

Figure S7. UV-vis-NIR absorption spectra of 100 μg mL^{-1} Ce-aMOFs and MEFs.

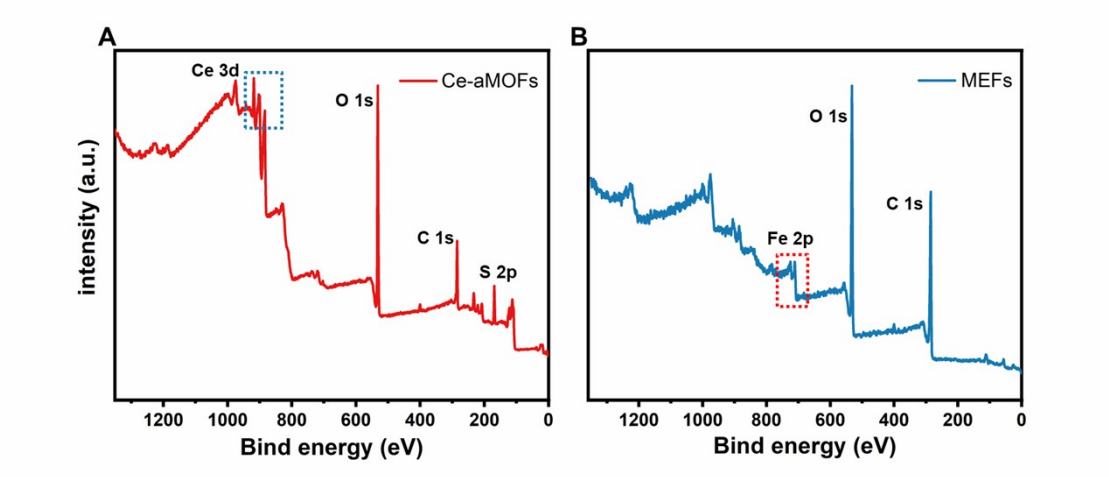

Figure S8. X-ray photoelectron spectroscopy survey spectrum of Ce-aMOFs and MEFs (Elements: C 1s, O 1s, S 2p, Cu 2p, Ce 3d).

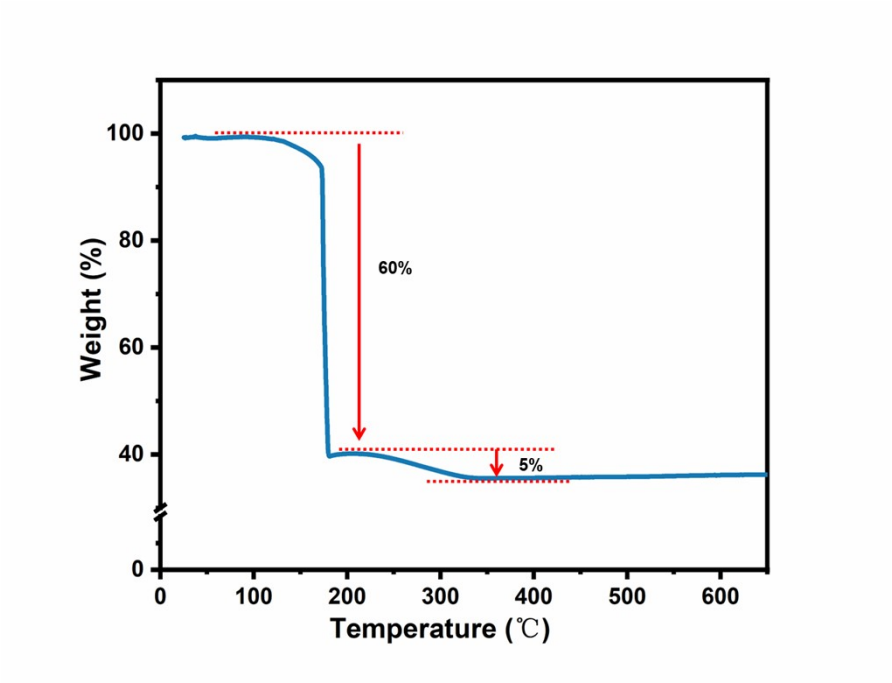

Figure S9. TGA analysis for MEFs in O_2 gas purging at a flow rate of 20 mL min^{-1}.

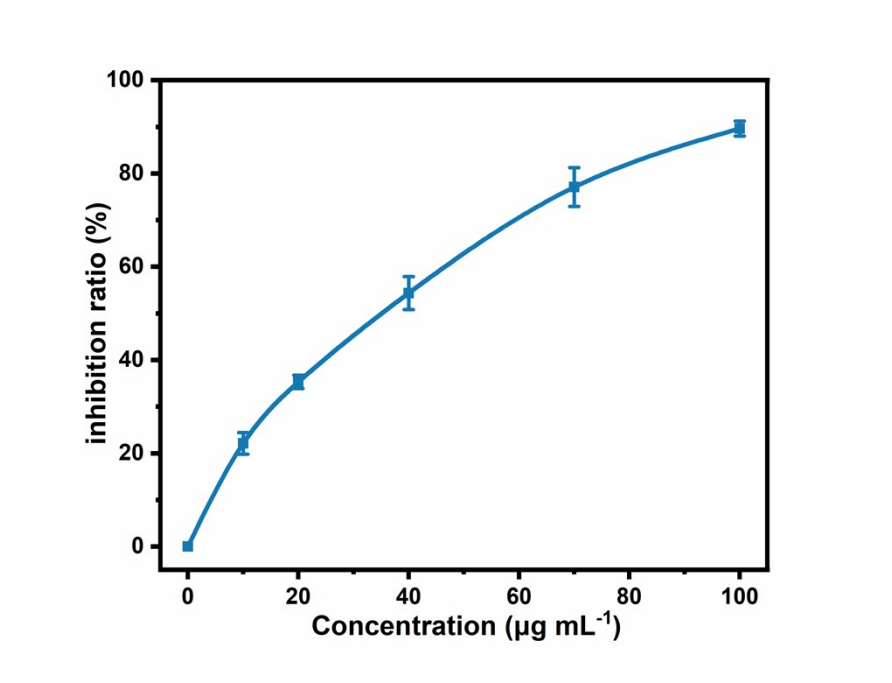

Figure S10. Inhibition rate of Ce-aMOFs (0-100 μg mL^{-1}) against the production of WST formazan.

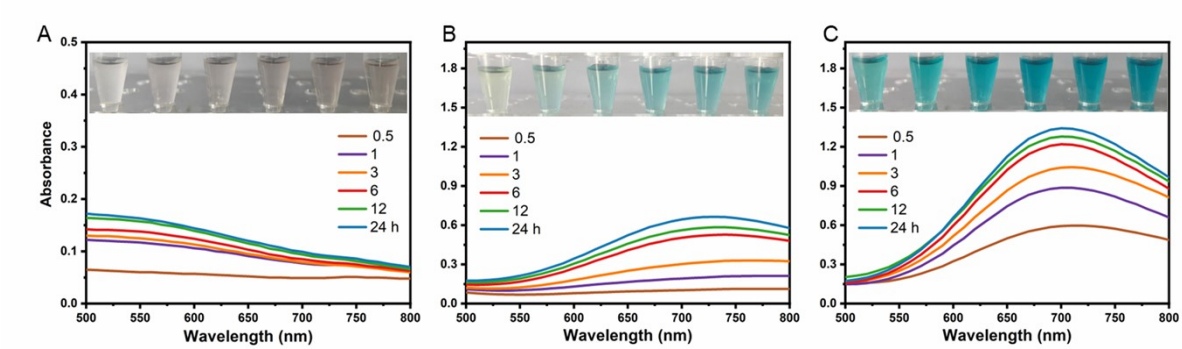

Figure S11. UV/vis-NIR absorption spectra of the MEFs solutions (200 μg mL^{-1}) after releasing Fe^{3+} at various pH values (A: pH 7.4, B: pH 6.5, C: pH 5.0). Inset: Prussian blue staining of the supernatant acquired at different incubation times.

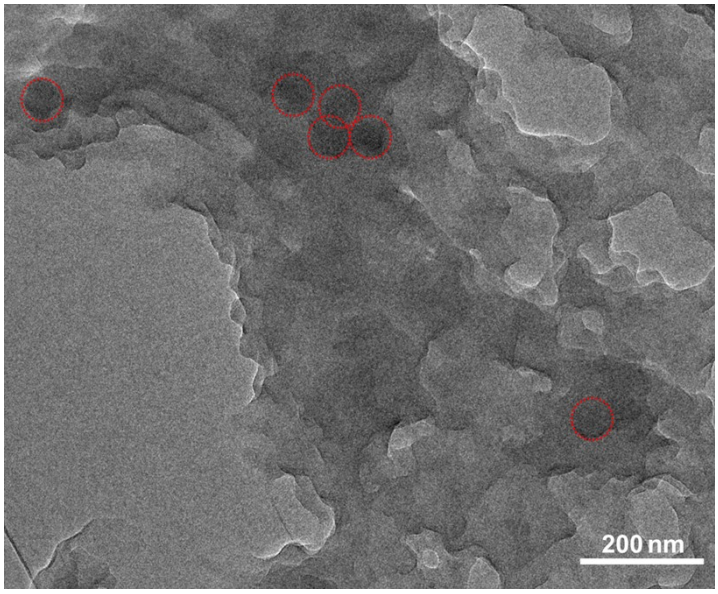

Figure S12. TEM image of MEFs degrading in pH 5.0 pbs for 12h, with a scale bar of 100 nm.

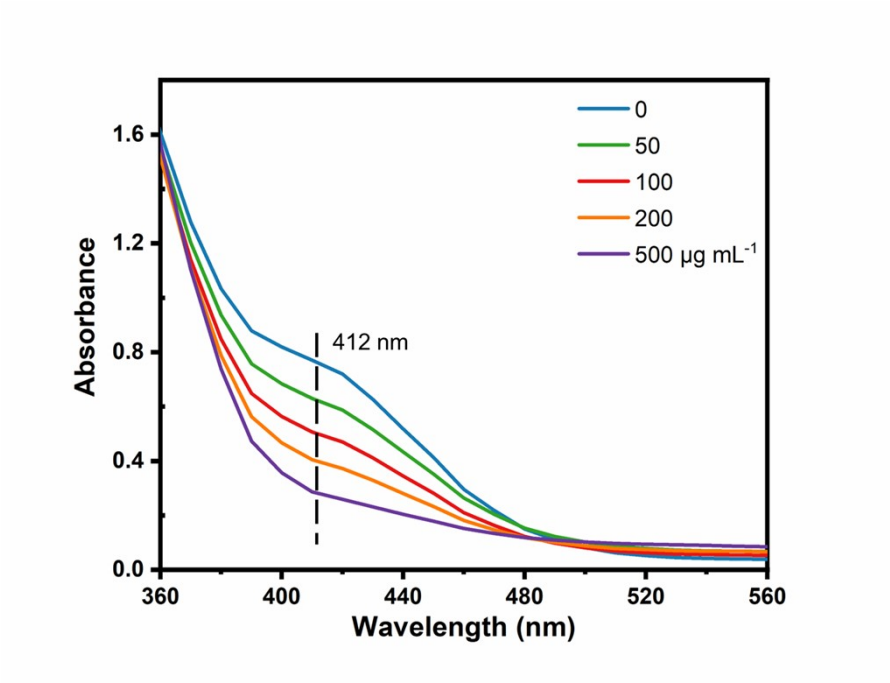

Figure S13. GSH depletion by MEFs with different concentration levels (0-500 μg mL^{-1}) in 8 h, as characterized by the absorbance at 412 nm.

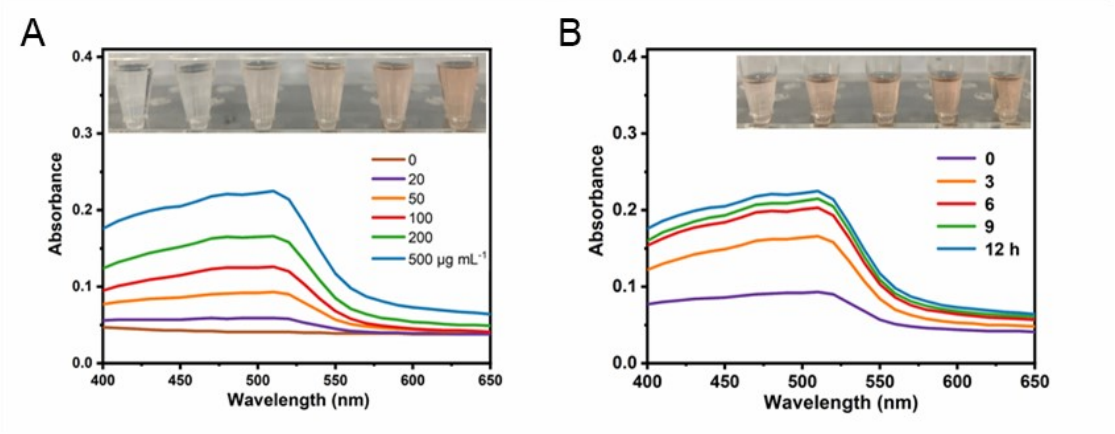

Figure S14. (A) The time-dependent production of Fe^{2+} from 500 μg/mL MEFs in the presence of GSH (5 mM). (B) The variation of UV/vis absorption spectra of the 1,10-phenanthroline hydrate-Fe^{2+} complexes after treatment with MEFs (0-500 μg mL^{-1}) for 6 h in an environment containing GSH (5 mM).

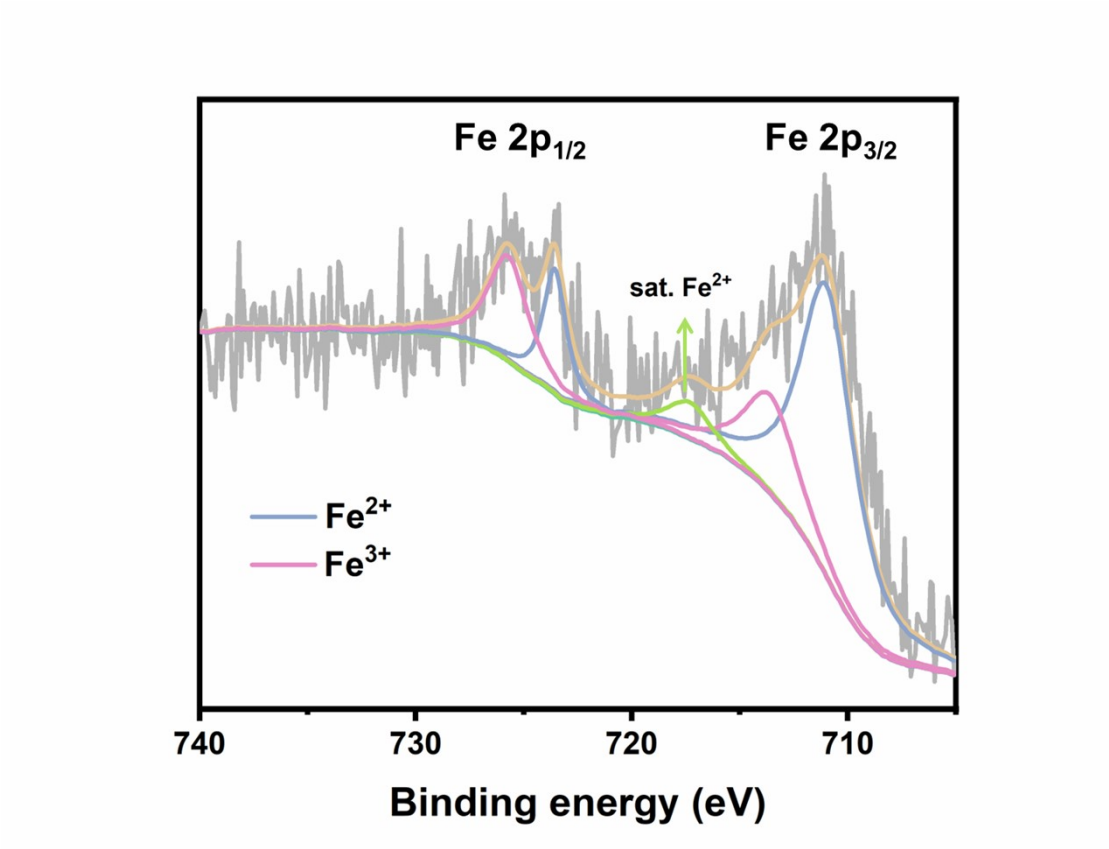

Figure S15. Valence status of Fe element in MEFs after reaction with GSH for 1h.

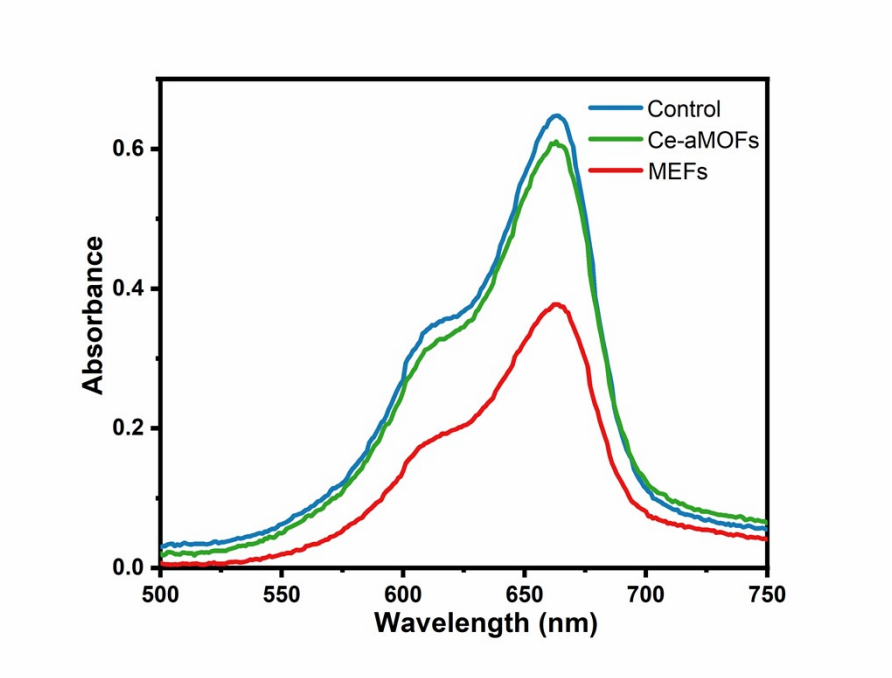

Figure S16. MB degradation by ·OH generated under 100 μg mL^{-1} Ce-aMOFs and MEFs with an incubation time of 2 h. Control group: GSH (100 μL, 1 mM), H_2O_2 (80 μL, 100 mM) and MB (10 μL, 100 μg mL^{-1}) in 500 μL aqueous solution.

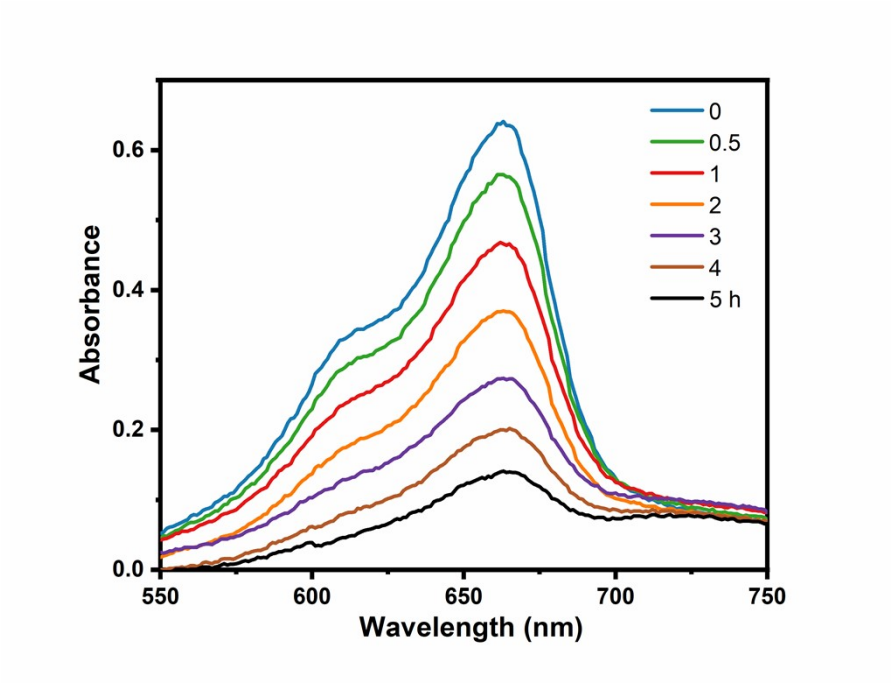

Figure S17. Degradation of MB by the MEFs-mediated Fenton-like reaction at different times with a concentration of 100 μg mL^{-1}.

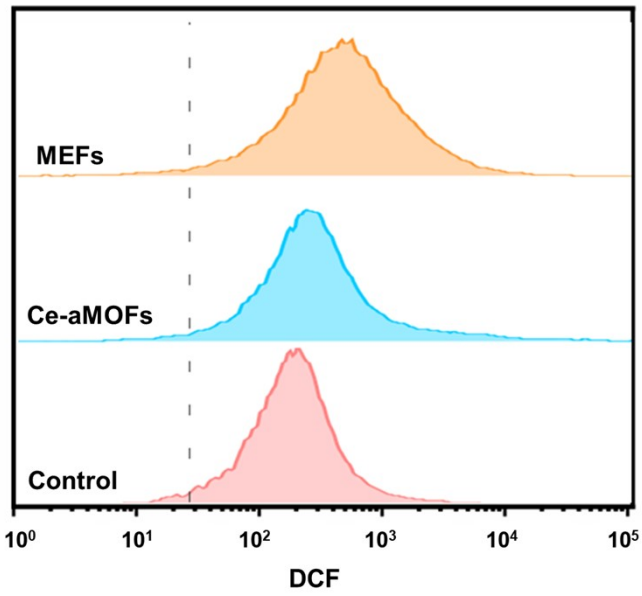

Figure S18. Flow cytometry analysis of ROS generation after treated with Ce-aMOFs and MEFs (100 μg mL^{-1}) for 8 h.

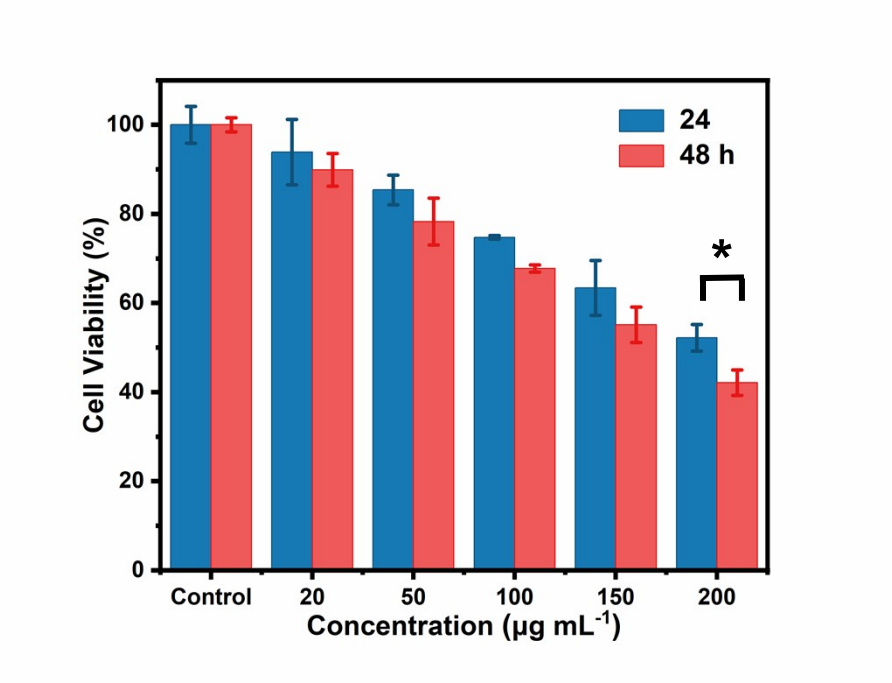

Figure S19. 4T1 cell viability after incubating with 20-200 μg mL^{-1} of Ce-aMOFs for 24 h and 48h.

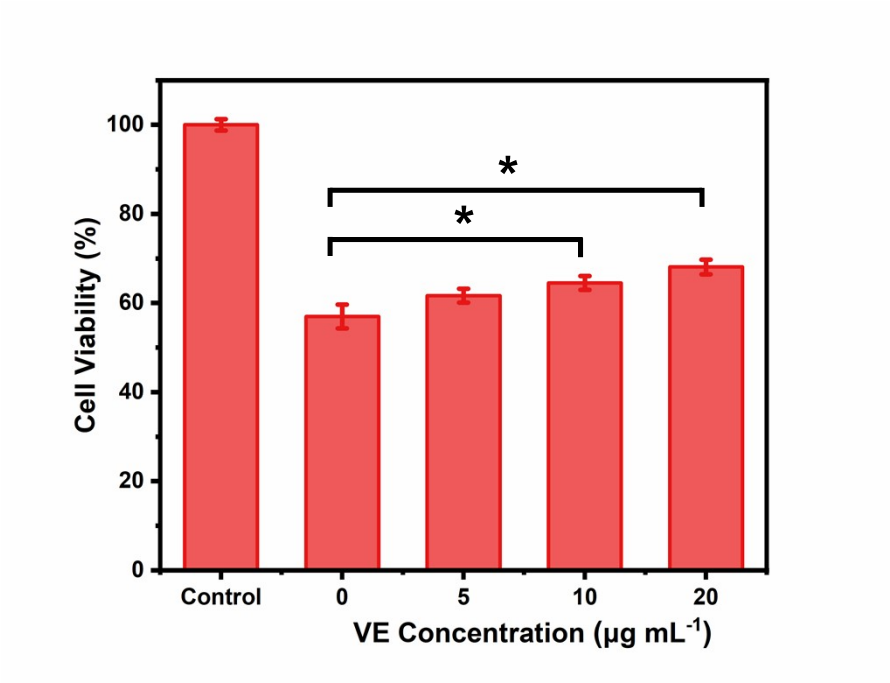

Figure S20. Relative cell viabilities of MEFs-treated 4T1 cells in the presence of vitamin E (VE).

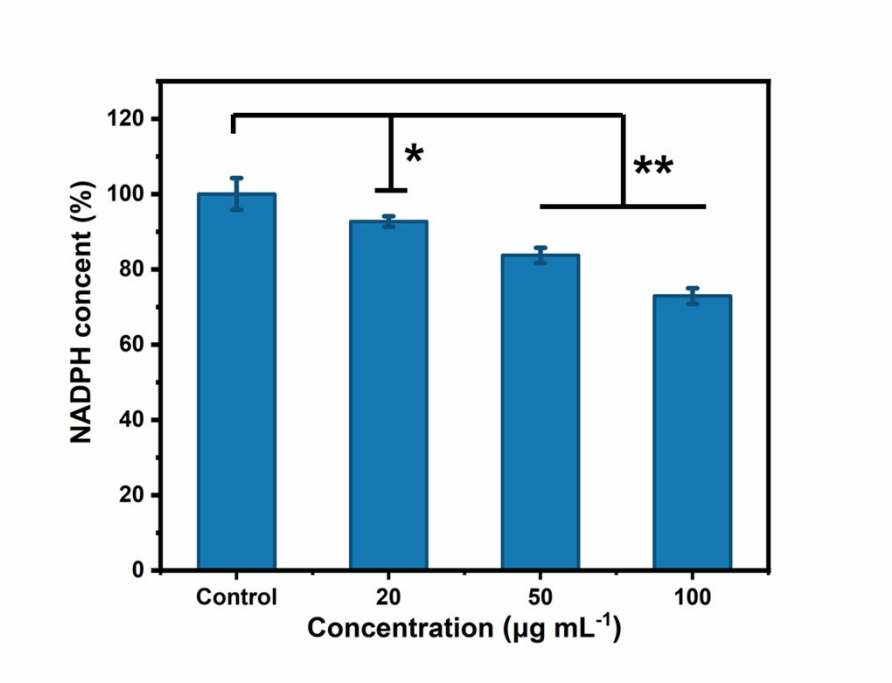

Figure S21. NADPH levels in 4T1 cells after treatment with Ce-aMOFs (20-100 μg mL^{-1}) for 6 h.

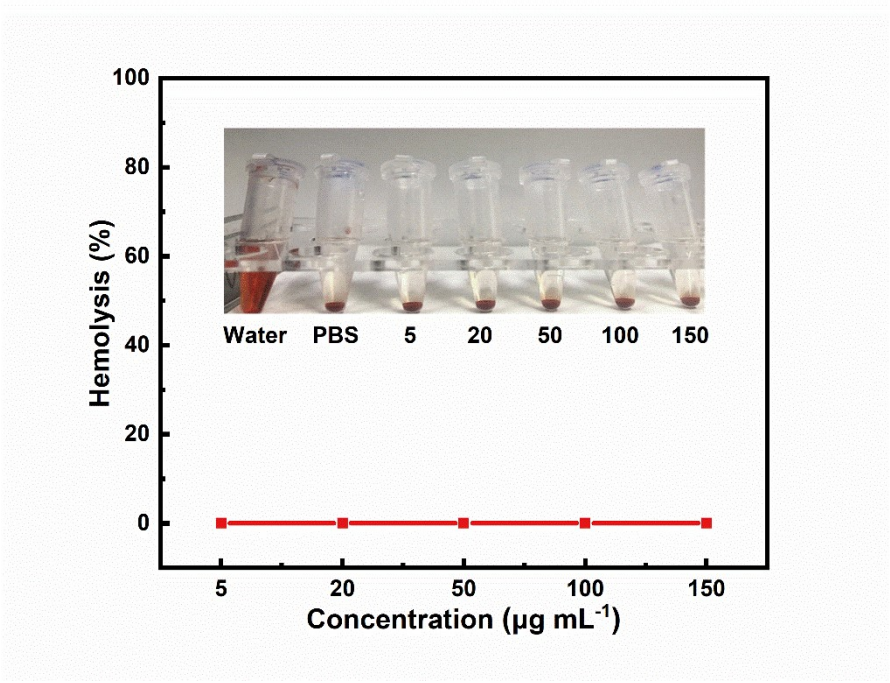

Figure S22. Hemolysis of MEFs (5-150 μg mL^{-1}) after incubation with red blood cells. PBS: negative control, deionized water: positive control. Inset: hemolysis photographs after centrifugation.

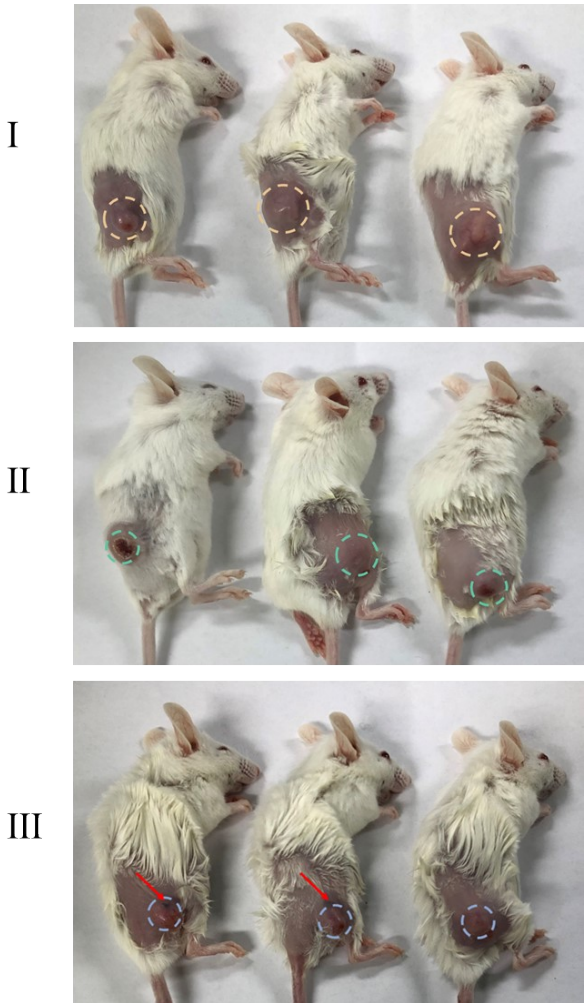

Figure S23. Photographs of 4T1 tumor-bearing mice from different treatment groups after 14 days of treatments. (I) PBS (pH 7.4, 10 mM, 50 μL), (II) Ce-aMOFs solution (2 mg mL^{-1}, 50 μL), (III) MEFs solution (2 mg mL^{-1}, 50 μL).

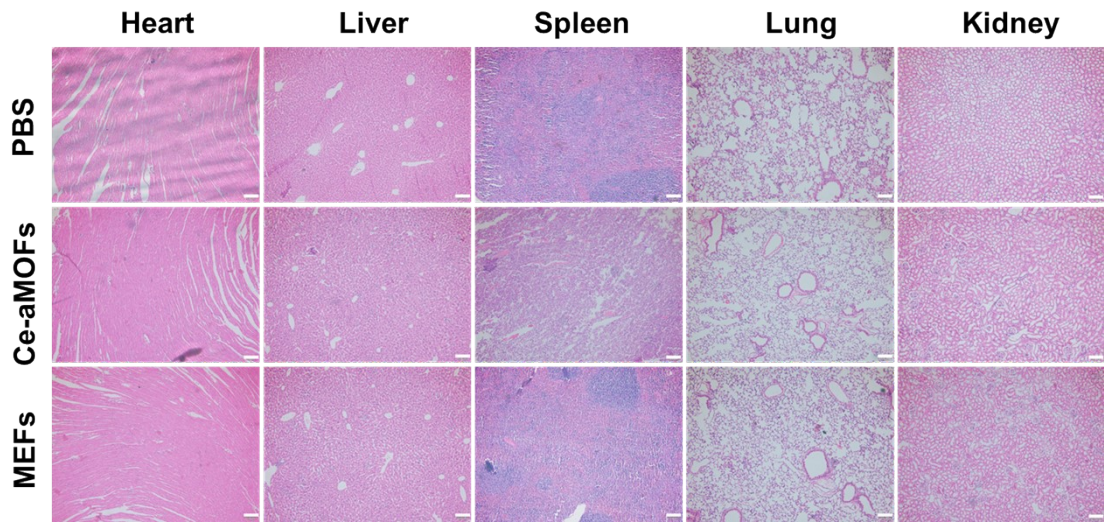

Figure S24. Images of H&E-stained major organ slices of mice from different treatment groups after 16 days of treatments. Scale bar 50 μm.